Bachelor Thesis - Electrical Engineering

Miniaturization and Characterization of a Ruthenium Oxide Potentiometric pH Sensor for Organs-on-Chip purposes

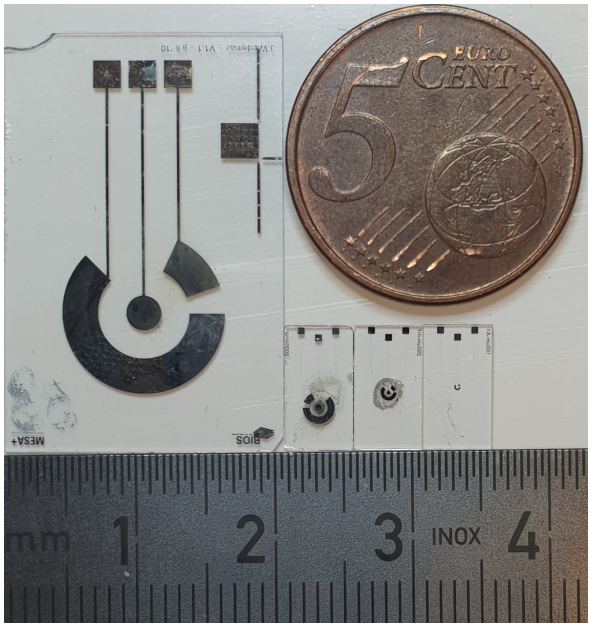

Sven van der Hoeven

S1600613

Members of the committee:

MSc. E. Tanumihardja
Dr.ir. W. Olthuis
Prof.dr.ir. A. van den Berg
Dr.ing. E.A.M. Klumperink

Date of publication: **November 19, 2019**

University of Twente
Faculty of Electrical Engineering, Mathematics and Computer Science

UNIVERSITY OF TWENTE.

BIOS Lab on a Chip group

Contents

1 Introduction

It really does sound futuristic, organs-on-chip(OoC). Nevertheless, this rather new technology of *in vitro* models of human tissue, promises to be more physiologically-relevant and ethical alternative to animal testing [1]. Moreover, it is a novel technique in contrast to regular *in vitro* processes used to develop new medications and therapeutic applications [2]. This technology comprises culturing human cells and tissue outside the body on chips, where the same environment is tried to be maintained as inside the human body, thus accurately replicating *in vivo* human physiology and pathology. This is realized by culturing the cells in small channels inside the chip, where micro fluids can be added or disposed with small pumps, creating an artificial circulation to provide the cells with all necessary nutrients. This enables researchers to personalize a OoC for a desired purpose, optimizing the model, for instance, investigating the effect of drugs or the cause of different diseases, etc. A optimized model makes this approach provide more realistic results in contrast to conventional *in vitro* methods [3–5].

However, one downside of this micro-environment is the low accessibility to monitor the behaviour inside the OoC, with for instance, a probe. One solution to this problem is the use of a micro-sensor. A micro-sensor enables accurate and non-invasive real-time monitoring of important parameters in OoC's [6]. On-chip pH sensors of metal oxide class, which are robust and long-lasting and more importantly, miniaturizable [7], could be used for long-term cell and tissue studies inside the OoC sensors. Many metal oxide electrodes show a linear response to proton concentration, but also often suffer from sensitivity to other oxidizing/reducing agents [8]. A necessary oxidizing agent, for organs-on-chips studies, which is always present, is dissolved oxygen. However, ruthenium oxide(RuOx) has been proven to be an exception to any significant effects on cross-sensitivity due to air oxidation, when moved from deoxygenated to oxygenated solutions [9]. This criteria is mandatory for a hypoxia study of cardiomyocytes, the first conceptualized use of a RuOx pH sensor in OoC studies. During this study, the oxygen levels in a medium are expected to vary between, a deoxygenated state, and a fully oxygenated state. In the first, cardiomyocytes are able to perform anaerobic glycolysis, resulting in a drop of 1-2 pH units in the surrounding medium. Because of the theoretical miniaturizability of Metal Oxide sensors it is expected that the macro-sized RuOx electrochemical sensor can successfully be scaled down without losing the characteristics of the macro-sized sensor developed by Tanumihardja et al. [9]. Therefore, in this work, the miniaturizability and transferability of the macro-sized RuOx electrochemical sensor is explored. If the micro-sized RuOx sensor proves the same characteristic behaviour such as, drift behavior, sensitivity, and response time, it can be integrated with an OoC used for the cardiomyocyte study.

1.1 Research Goals

This project is aimed to first study the miniaturizability and transferability of the macro-sized RuOx electrochemical sensor. Then designing, fabrication and characterization of the sensor will follow.
This can be broken down into the following sub-research aims:

- To determine the electrode design capable of electrochemical sensing and performing different characterization tests
- To fabricate on-chip sensors
- To characterize the electrochemical sensing chip
- To determine the limits of the fabrication process

1.2 Thesis Outline

In chapter 2, the terms and concepts necessary to describe electrode reactions are introduced. Followed by the design in chapter 3, explaining all design considerations. All experimental protocols for both the fabrication process and on-chip characterization setup are discussed in chapter 4. All results and findings regarding the fabricated chips are presented and discussed in chapter 5. Finally, in chapter 6, conclusions are drawn and recommendations are given for future use of the sensor.

2 Theory

2.1 Introduction to Electrochemistry

As the word electrochemistry already reveals, it is the branch of chemistry where there is a relation between electrical and chemical effects. A large part of this field deals with the study of chemical changes caused by the passage of an electric current and the production of electrical energy by chemical reactions. With the help of electrochemisty one can do, for instance, electroanalysis, store energy, electrodeposition, electrosynthesis and electrolysis. The main technique of electrochemistry used in this work is electroanalysis, which is explained later in this chapter. But first, an electrochemical cell is introduced below.

2.2 Electrochemical Cells and Reactions

In electrochemical systems, we are concerned with the processes and factors that affect the transport of charge across the interface between chemical phases, for example, between an electronic conductor (an electrode) and an ionic conductor (an electrolyte). However, a current only can flow if the circuit is closed. If this single interface is extended to two electrodes, separated by at least one electrolyte phase, the circuit can be closed and can be described as an electrochemical cell, this situation can be seen in figure 1. The chemical reaction taking place in the cell, which describe the chemical changes happening at the two electrode-electrolyte interfaces is called an oxidation-reduction reaction (redox-reaction). Oxidation and reduction reactions always occur as a pair, therefore each half-reaction at the surface of each electrode can be denoted by:

$$C_{ox} + ne^{-} \rightleftharpoons C_{red} \tag{1}$$

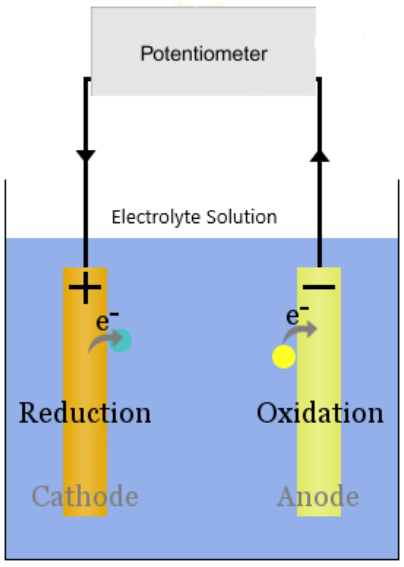

Figure 1: A basic electrochemical cell: A redox reaction results in a potential difference between the anode and the cathode.

From equation 1 it is apparent that there is an electron transfer, between the reducing agent, providing the electron by undergoing oxidation, and the oxidizing agent by undergoing reduction. The resulting electrical charge is proportional to the mass (m) and the molecular weight (MW) of the converted chemical, n is the moles of electrons, and F is Faraday's constant.

$$Q = \frac{nFm}{MW} \tag{2}$$

When positive charge flows out into the electrolyte, the electrode is defined as the anode. Where the anode current is generated due to the oxidation reaction. On the other hand, when the charge flows

from the electrolyte into the other electrode, the cathode, it is called the cathodic current accordingly, which is then due to the the reduction reaction. The Gibbs free energy ΔG necessary to move the charge, Q, over a certain potential E is given by

$$\Delta G = EQ \tag{3}$$

with n the amount of moles of electrons/mole of reactant, the change in Gibbs free energy for a redox-reaction is

$$\Delta G = -nFE \tag{4}$$

substituting equation 4 in the formula for Gibbs free energy in equilibrium state, which is given by

$$\Delta G = -\Delta G^0 + RTln\frac{C_{ox}}{C_{red}} \tag{5}$$

with T the temperature, and R the universal gas constant, results in

$$-nFE = -nFE^0 + RTln\frac{C_{ox}}{C_{red}} \tag{6}$$

dividing both sides of equation 6 by -nF, brings us to the Nernst equation

$$E = E^0 - \frac{RT}{nF}ln\frac{C_{ox}}{C_{red}} \tag{7}$$

The Nernst equation (eq.7) provides a link between the electrode potential and the concentrations (activity) of the chemical elements in the half-reaction. If a system follows the Nernst equation, or an equation derived from it, the electrode reaction is electrochemically reversible (or the reaction shows nernstian behaviour).

2.3 Two Main Electroanalytical Techniques

A distinction can be made between two main types of interfacial electrochemical techniques.

- Static techniques: No current flows at an equilibrium potential
- Dynamic techniques: The current that flows at an applied potential is measured, or vice-versa, the potential is measured, at an applied current

All common static and dynamics techniques are depicted in figure 2.

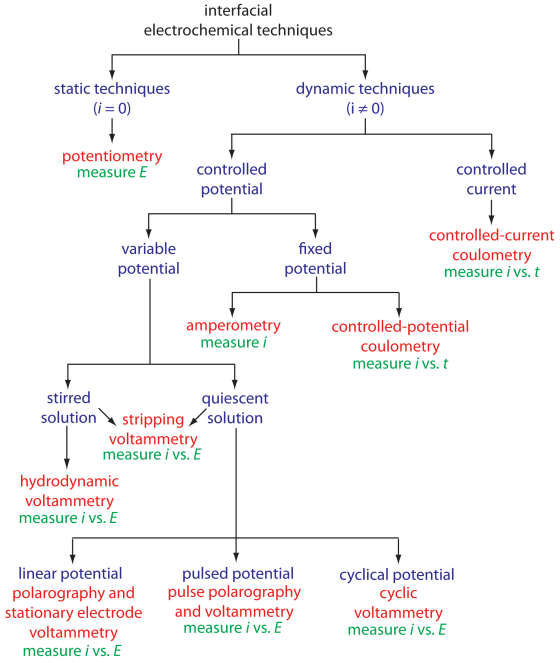

Figure 2: All common interfacial electrochemical techniques

2.3.1 Static techniques

As mentioned earlier, the electric potential only occurs at the electrode-electrolyte interface. Moreover, we see that the electrode potential is not linked to any dimensions of the electrode nor linked to any kinetic reaction parameters. Resulting that the potential and the surface concentrations are always kept in equilibrium with each other by fast charge-transfer processes [10]. This means that both electrodes have an equilibrium potential, given by the Nernst equation (eq.7). This also means that practically no current runs through the system, and therefore the composition of each electrode also stays the same, enabling us to use it as an electroanalytic method [11].

Potentiometry

In this project the static technique called potentiometry is used. In potentiometry the potential between two electrodes of an electrochemical cell, which is at equilibrium, is measured. In electrochemical sensors, only one electrode is in direct contact with analyte solution, so, direct change in potential only happens at this interface, this electrode is called the indicator, or working electrode (WE). The other electrode is known as the reference electrode (RE), which should have a known fixed potential. Now, the difference between the two potentials can be measured with a potentiometer (potentiostat). The potentiometer should have a huge internal resistance (in the $G\Omega$ range) to ensure (almost) no current flows. With the setup shown in figure 8, different potentials at the working electrode can thus be measured.

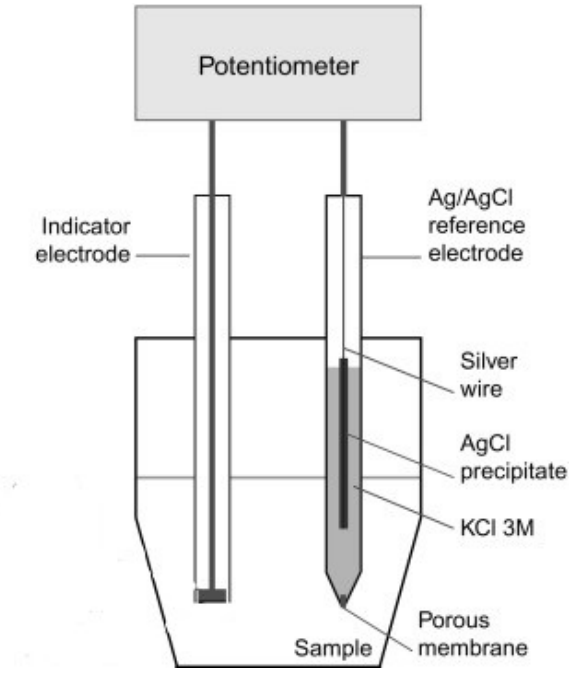

Figure 3: A basic electrochemical sensor setup

2.3.2 Dynamic techniques

If an external potential is applied, the potential is moved away from equilibrium position. As a direct result, current then flows as the system moves toward a new equilibrium position. At first the initial current is large, but it decreases over time eventually reaching zero when the reaction is at equilibrium again. The current, therefore, changes in response to an applied potential. Vice-versa, a fixed current can be passed through the electrochemical cell, forcing the concentrations of the electrolyte to change, thus forcing a potential. If the Nernst equation is rewritten to

$$C_{ox}/C_{red} = e^{(E_{appl} - E^0/(RT/nF))} \tag{8}$$

the link between concentrations and applied voltage is directly made clear. Due to the high initial current it is implied that a very strong electric field exists at the interface, and it can be expected

that this field exerts its effects on the behavior of electrons and ions in the electrode-electrolyte interface [11]. Also, the magnitude of the potential difference at an interface has an effect to the relative energies of the carriers in both the electrode and the electrolyte. This means the potential controls the direction and the rate of charge transfer. Thus, the measurement and control of cell potential is one of the most important aspects of experimental electrochemistry [10]. However, in this project no dynamic techniques will be used for electroanalytic methods. Therefore no in-depth analysis, regarding dynamic techniques, will be given in this work, except for the two below, which do get used in this work.

Electrodeposition

Electrodepositon can be seen as a reversed battery, instead of getting a current from the cell, a current is forced through the cell, forcing a redox reaction, on each electrode according to equation 9 (one way at each electrode). The goal of electrodeposition is to cover the cathode by a layer of metal ions, which come from the surrounding electrolyte solution, called a bath, or from the anode, which then corrodes by releasing metal ions. [12]. In fig.4 a graphical representation is given how a spoon can get a layer of silver ions.

$$Ag^{+}_{(aq)} + ne^{-} \rightleftharpoons Ag_{(s)} \tag{9}$$

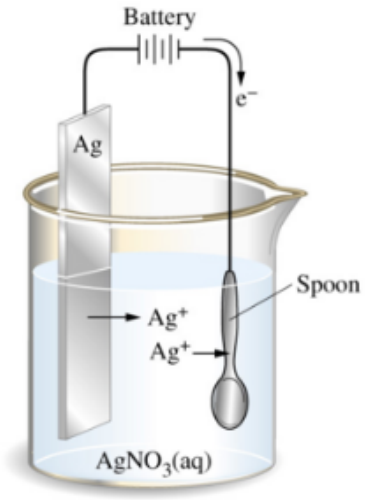

Figure 4: A basic electroplating setup: a current is applied to move Ag^{+} ions from the anode (oxidation reaction), to the cathode (reduction reaction)

Electrochemical cleaning

On the other hand, instead of covering an electrode with a layer, the process can also be used to first, remove the top layer of an electrode and then, re-grow the top layer. This process is repeated several cycles, to "clean" the electrode from dirt and contaminates on the surface.

Ohmic drop

If dynamic techniques are used, current flows and results in a voltage drop equal to $i(R_s + R_w$, whereas R_s is the solution resistance between the electrodes and R_w is the resistance in the wires. If R_s is high, or if too much current flows through the reference electrode, the concentration of ions changes, resulting in a potential shift. This potential shift has significant influence on electroanalytical measurement results. One way to reduce the ohmic drop R_s, is by decreasing the distance between working and reference electrode, which happens by nature with (ultra)micro electrochemical cells, or to use a counter electrode, which is explained in 2.4.3.

2.4 Electrodes

2.4.1 Working electrode

In this project RuOx is used as the working electrode (WE). The chemical reaction of RuOx occurring has the form of

$$RuO_x(OH)_y + ze^- + zH^+ \rightleftharpoons RuO_{x-z}(OH)_{y+z} \tag{10}$$

Which can be simplified to

$$Ru^{IV}O_2 + e^- + H^+ \rightleftharpoons Ru^{III}O(OH) \tag{11}$$

The simplified reaction filled into the Nernst equation (eq.7) will give the relation to the pH value

$$E = E^0 - \frac{RT}{F} ln \frac{c(Ru^{III})}{c(Ru^{IV}) \cdot c(H^+)} = E^0 - \frac{ln10 \cdot RT}{F} log(\frac{c(Ru^{III})}{c(Ru^{IV}) \cdot c(H^+)}) \tag{12}$$

Filling in the temperature, Faraday's constant, the universal gas constant, and removing the log, results in

$$E = E^0 - 0.0586V \cdot pH, (22°C) \tag{13}$$

where the thermodynamically calculated standard potential (vs Ag/AgCl in sat'd KCl) equals $E^0 = 0.777V$ [13–15]. According to equation 13, a linear response to pH can thus be obtained using RuOx as WE.

2.4.2 Reference electrode

For the reference electrode(RE), the primary reference is the standard hydrogen electrode (SHE) which has been agreed to have a standard potential of $E^0 = 0.00V$. However, SHE is not practical in use, let alone the ability to miniaturize a SHE is complicated and unnecessary. Therefore, another common reference electrode, the silver-silver chloride electrode, is used in this project. The Ag/AgCl RE typically is a Ag wire with a AgCl coating, all packed in a Cl^- rich electrolyte solution and a membrane, to allow a salt-bridge between two different electrolyte solutions. The according redox reaction is as follows

$$AgCl_{(s)} + Ag_{(s)} + e^- \rightleftharpoons Ag_s + e^- + Cl^- + Ag^+ \tag{14}$$

which can be simplified to

$$AgCl_{(s)} + Ag_{(s)} \rightleftharpoons Ag_s + Cl^- + Ag^+ \tag{15}$$

filling the redox reaction into the Nernst equation (eq.7)

$$E = E^0 - \frac{RT}{nF} ln(C_{Cl^-}) \tag{16}$$

the reported standard potential for a Ag/AgCl electrode in saturated KCl solution vs SHE is $E^0 = 0.1997V$ [16]. The advantage of an Ag/AgCl RE is that it can be made very small and integrated in micro-chips. The only difference is that the Ag/AgCl wire is made without the separate Cl^- rich solution and is, just like the WE, in one analyte solution. If we look at equation 16, it can be seen that the potential is depended on the Cl^- concentration in the analyte solution and therefore has no fixed potential anymore, it is therefore called, a quasi-reference electrode(QRE).

2.4.3 Counter electrode

Another electrode, called the counter electrode(CE) can be added to the two electrode cell. When dynamic techniques are used, the CE allows current to run between WE and CE without interfering with the RE, which should maintain a fixed potential.

However, this does mean that the CE needs to be made from an inert material, so it does not get involved in any chemical reactions, and its size should be much larger than the working electrode to ensure no current limiting situations arise [17].

3 Design

3.1 Design electrode dimensions

Based on the theory for potentiometry, electrode dimensions should not have any significant influence to the sensor's sensitivity. To experimentally confirm the effect of miniaturization on the macro-sized sensor's sensitivity, it was chosen to have exact scaled-down versions of the macro-sized RuOx sensor electrodes, resulting in the dimensions according to table 1. To verify that geometry of the electrodes indeed do not play a role, working electrode rods, in contrast with the circular shape of the macro-size WE, with different lengths and widths comparable to the specified WE area, are made in addition to the scaled versions. Also WE area influence was checked by adding an 500 micron WE array. Both alternative mask can be seen in figure 7a and 7b.

3.2 Design chip holder

Moreover, a teflon chip holder with 1mL reservoir was available for use (see figure 5). The reservoir has small hole with a diameter of 3.5mm in the bottom were the active elements of the chip can be exposed to an analyte solution. The chip holder was able to fit glass chips measuring 9mm x 5mm x 525µm(l x w x h), and was enhanced with 0.5mm pogo pin connectors to make a connection with a potentiostat.

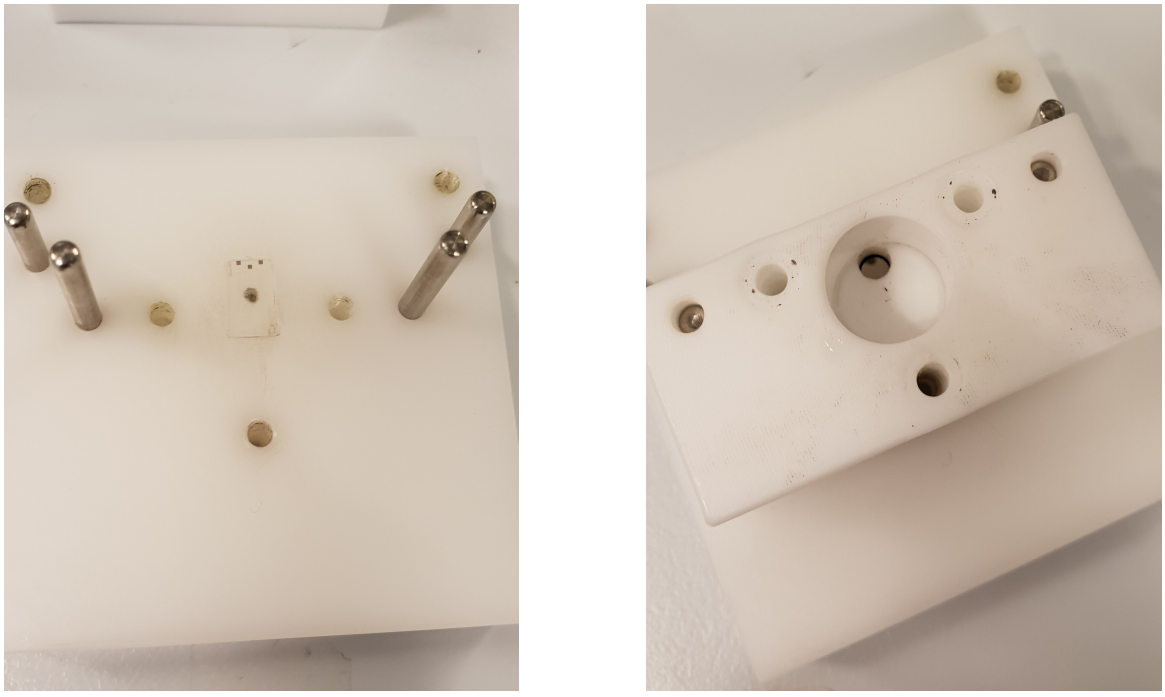

(a) Teflon base, with a RuOx chip mounted

(b) Teflon Reservoir mounted to base

Figure 5: Teflon chip holder design

3.3 Design mask

Each single chip is thus bounded by the chip holder fitting and the mask was designed accordingly, two examples of 250 and 500 micron can be seen in figure 6a and 6b. The blue color represents the only mask layer, which is gonna be a Pt layer, which is the same as the macro-sized sensor and an inert metal. The red circle is the active electrode area exposed to analyte solution, and is only a drawing aid. The WE array in 7a has the same radius as the 500 micron array in 6b but smaller WE area due to the array like structure. The Pt rectangles around the chip are removed during the cutting process to make individual chips. The resolution of the sputtering process is 3 μm.

Chip name	WE area (µm)	WE Area compared to macro-sized (%)	WE diameter(µm)
Macro-sized	4908738,521	100	2500
500 micron	196349,5408	4	500
250 micron	49087,38521	1	250
100 micron	7853,981634	0.16	100
50 micron	1963,495408	0.04	50
25 micron	490,8738521	0.01	25
10 micron	78,53981634	0.0016	10

Table 1: Planned dimension of miniaturized sensors

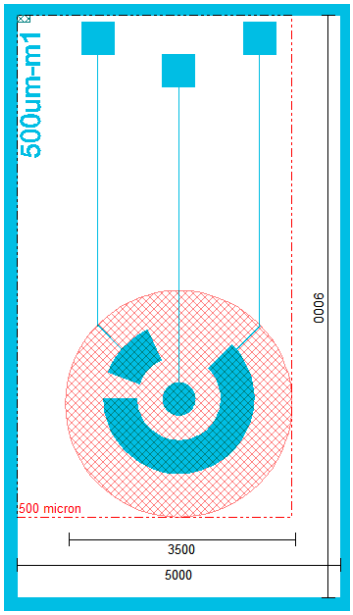

(a) 500 Micron

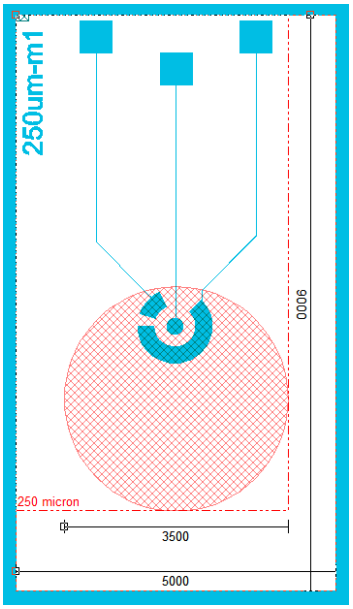

(b) 250 Micron

Figure 6: Mask designs of scaled versions

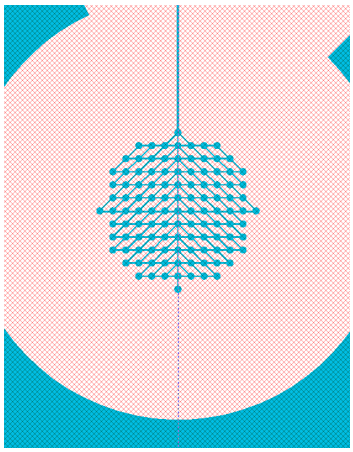

(a) 500 Micron array

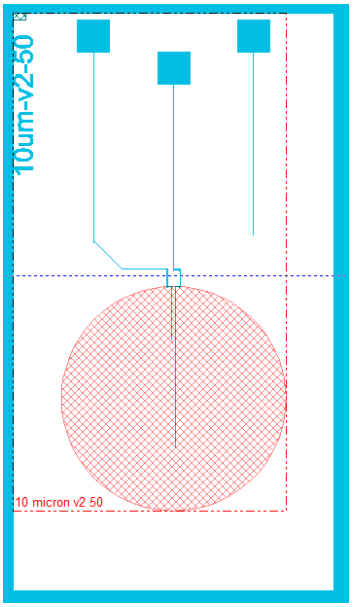

(b) 10 Micron rods

Figure 7: Alternative mask designs

4 Experimental

4.1 Introduction

To have a comparison with the macro-sized RuOx sensor, all procedures, to fabricate and characterize the micro-sized RuOx sensor will be analogous to the ones described by Tanumihardja [9]. An attempt will be made at carrying out each experiment protocol until it is no longer feasible, then different protocols will be tested.

4.2 Ruthenium Oxide Sensor Fabrication

First, according to the mask from the design section the circular and hemispherical Pt electrodes were sputtered on a glass wafer. The wafer was then cut in individual chips measuring 9 by 5 mm each. Each chip was first cleaned, which will be explained next, and individually processed further. Two main methods were used to fabricate RuOx nanorods on the electrodes, a drop-casting production method and electrodeposition.

4.2.1 Cleaning the chips

The Pt working electrode of each chip was first electrochemically cleaned before being used as RuOx substrate by applying cyclic potential sweeps for at least 20 cycles, with a scan rate of around 100 mV/s in 0.5 M sulphuric acid between 0.6 and 1 V (vs. Ag/AgCl). Additional cleaning processes were sometimes used as pre-treating for electrodeposition or the drop-casting production method. These processes comprised of, etching with acids, rinse with acetone, roughen up the Pt electrodes with sand paper and degrease with soap and de-ionized water(DI-water).

4.2.2 Drop-casting production method

The main RuOx electrodes used in this project were made by using a $Ru(OH)_3$ precursor, according to the protocol of Chen et al. [18], which was then precipitated in DI-water, with different concentrations. The precursor suspension was pipetted directly onto the working electrode of a cleaned chip. Scotch tape was used to shield the rest of the chip from precursor solution, and it was then left to dry at room temperature enabling the solvent to evaporate. The drop-casting processed chips where annealed at $350°C$ in a preheated oven for around 3 hours. As confirmed by other works [9, 18] RuOx nanorods can be formed after annealing.

Another batch was made, using a $Ru(OH)_3$ precursor which was more concentrated. This was done by centrifuging the solid $Ru(OH)_3$ solution. Due to centrifuging the $Ru(OH)_3$ separated in a $Ru(OH)_3$ pallet on the bottom, and the supernatant on top. A pipet was injected inside the pallet, sucking the pallet from the solution, and then directly apply the pallet onto the active Pt parts of the chip (not specific on the WE only). This was done to ensure all WE's had a substantial amount of $Ru(OH)_3$ precursor on them. Again, the excess solvent was left to evaporate at room temperature, but in contrast with the oven, this batch of chips was heated on a $300°C$ hotplate for 5 hours.

4.2.3 Electrodeposition

A few RuOx chips with sub 50 micron diameter WE's, were modified through electrodeposition, to accurately fabricate RuOx WE's, without contaminating the RE or CE with RuOx. Cleaned chips were put in the chip holder and heated to 50-60$°C$ au bain-marie. The reservoir was filled with pre-heated 50mM $RuCl_3$ with and without adding extra sulphuric acid. A Pt wire was put in the reservoir and used as reference electrode whilst an internal Pt electrode was used as counter electrode. Chronoamperometry was then used to apply -0.93V for around 3 minutes as pre-oxidation step, and -0.2V for approximately 30 minutes to built a few µm thick layer. The chips were dried at room temperature and then annealed at 150 °C.

Moreover, electrodeposition was also used to fabricate quasi-Ag/AgCl reference electrodes. Cleaned chips were put in the chip holder and the reservoir was filled with 0.3M $AgNO_3$ in 1M NH_3 solution.

Chronoamperometry was then executed, using Ag wire as quasi-reference electrode and the on-chip Pt counter electrode. After an Ag layer was plated, the reservoir was cleaned and filled with a 1M KCl solution used to chloridize the Ag layer by applying a small current (∼40nA) for 20 minutes.

4.3 Measurement setup

The standard measurement setup was according to figure 8. A RuOx chip is put in the chip holder, and an external commercial grade Ag/AgCl (sat'd KCl) liquid-junction RE from CH instrument, is put in the reservoir. The potential is then measured between the WE and RE according to protocols from section 4.4. Potentials were measured using a Bio-Logic SP300 bipotentiostat, with an internal resistance $>100G\Omega$. During all measurements the whole setup was also placed inside a metal box, which acted as a Faraday cage, to reduce external noise. Before any solution was put in the reservoir and measurements were conducted, the solutions were checked with a Mettler-Toledo pH meter, which was calibrated with IUPAC certified buffer standard solutions of pH 4.005, 7.000 and 10.012, and the temperature was noted.

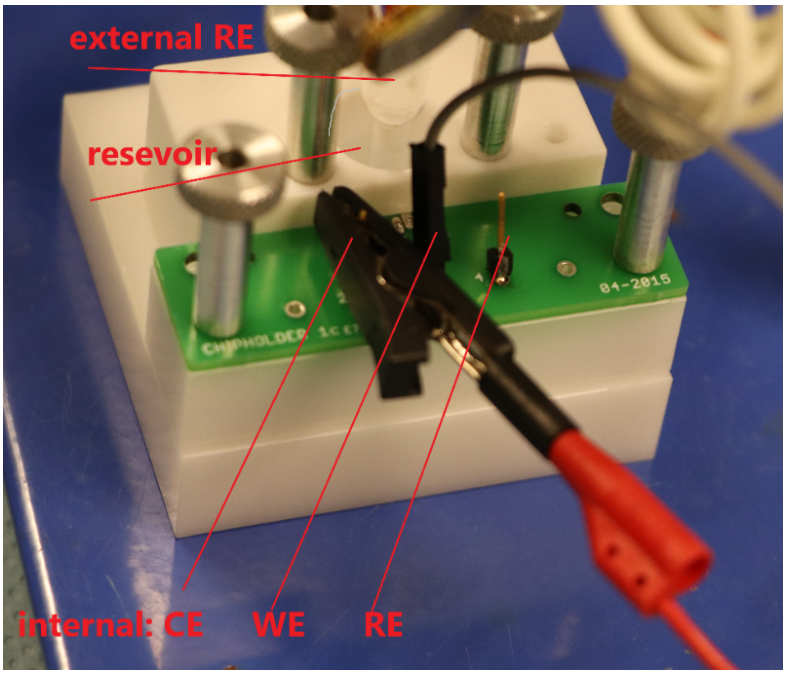

Figure 8: Measurement setup: WE and RE connected to potentiostat

4.4 Measurement Protocols

4.4.1 Open circuit potential vs (standard) pH buffers

All open circuit potential(OCP or OCV) measurements were recorded for 120s at 0.5s intervals. Where the potential at 120s was noted for pH response calculations. The first measurements were performed with the standard buffer solutions also used to calibrate the pH meter. For each RuOx chip of the first batch, measurement iterations of pH 4,7 and 10 solutions, were conducted in random order. Before a different pH solution was put in the reservoir, the reservoir and RE were rinsed with DI-water and dried with paper.

For the second batch of RuOx chips, The pH range was then extended with pH 5 buffer solution, consisting of acetic acid/sodium acetate, pH 8 buffer solution, consisting of monopotassium phosphate/disodium phosphate, and pH 2 buffer solution, consisting of KCl/HCl.

4.4.2 Open circuit potential vs drift time and influence of oxygen

Drift measurements >120s were conducted with phosphate-buffered saline (PBS) buffer with pH 7,4 at 21°C. Drift was then calculated by applying a linear fit to the slope.

The dependence on oxygen was tested with oxygen enriched PBS and deoxygenated PBS. This was done by saturating the PBS with air, by purging instrument air through the PBS for $\sim 1h$. Deoxygenated PBS was made by purging argon gas through the PBS for $\sim 1h$. Both purgings were done with the setup used in figure 9, releasing the particular gas at the bottom of the container through a needle, which forced the selected gas back through the liquid inducing bubbles, removing or trapping oxygen. Again, drift was then calculated by applying a linear fit.

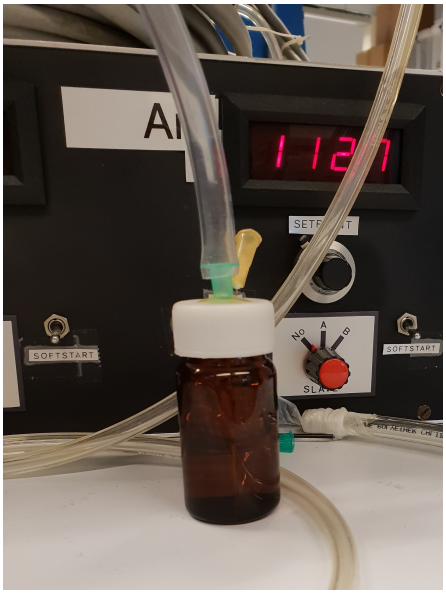

Figure 9: The purging setup: green cap = inlet, yellow cap = outlet

4.4.3 Open circuit potential response time

To test the response time, the reservoir was half-filled (0.5ml) with 20mM KH_2PO_4, 5mM KCl and 137mM $NaCl$. The open circuit potential recording was then started to form a base plateau potential. After 50 sec 0.5M K_2HPO_4 was pipetted to fill up the rest of the reservoir (0.5ml). When a new potential plateau was formed, the recording was stopped and the time between the base plateau and new plateau was noted as the response time. This experiment was repeated with applying both solutions in different order.

4.4.4 Open circuit potential of quasi-Ag/AgCl vs Cl^- concentration

To calibrate the OCP response vs Cl^- concentration of the quasi-Ag/AgCl reference electrode(QRE), solutions with different concentrations of Cl^- were made by diluting 1M KCl with DI-water. The known Cl^- solutions were then pipetted in the reservoir and the QRE OCP was measured against a commercial grade Ag/AgCl(sat'd KCl) reference electrode. The OCP was noted after 120s. The known Cl^- concentrations in the solutions are linked with the OCP measured. A linear fit was then applied to determine the slope in mV/-log[Cl^-].

4.4.5 Ohmic drop

Potentio Electrochemical Impedance Spectroscopy (PEIS) was used to obtain a Nyquist plot. The ohmic drop was then determined from a Nyquist plot by looking at the real part of the impedance for a frequency of 100khz.

5 Results and Discussion

5.1 Fabrication

5.1.1 Drop-casting production method

All RuOx chips were checked for RuOx growth, under the microscope and scanning electron microscope(SEM). The first batch according to the protocol of Tanumihardja [9], showed a shiny glow under x5 magnification after evaporating the solvent. After annealing, the $Ru(OH)_3$ precursor turned into flat, mud-crack like island, of RuOx depicted in figure 10. When a closer look is taken with the SEM, the morphology was shown (see fig.11), a porous amorphous/crystalline structure of nanospheres with diameter of a few nm was found.

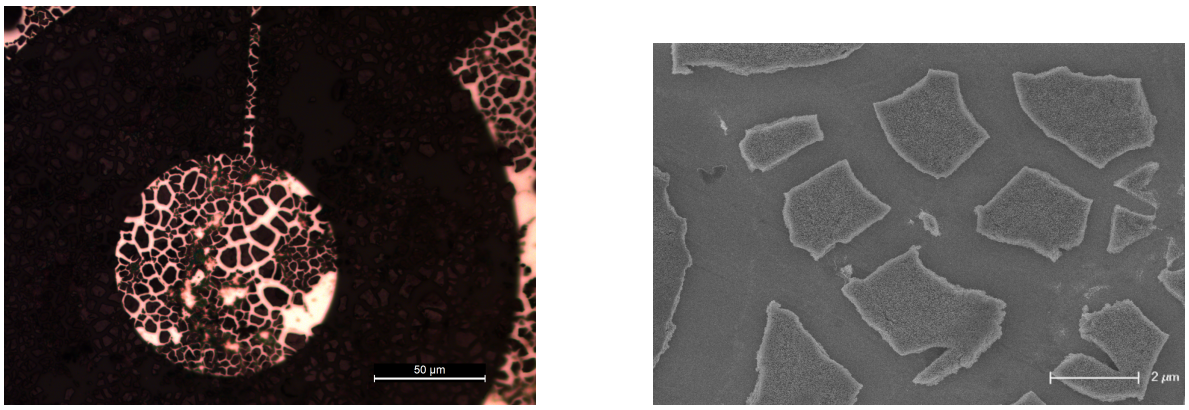

(a) Using normal microscope: Dark-field + polarization filter at 10x magnification

(b) Using SEM

Figure 10: Mud-crack island RuOx batch 1

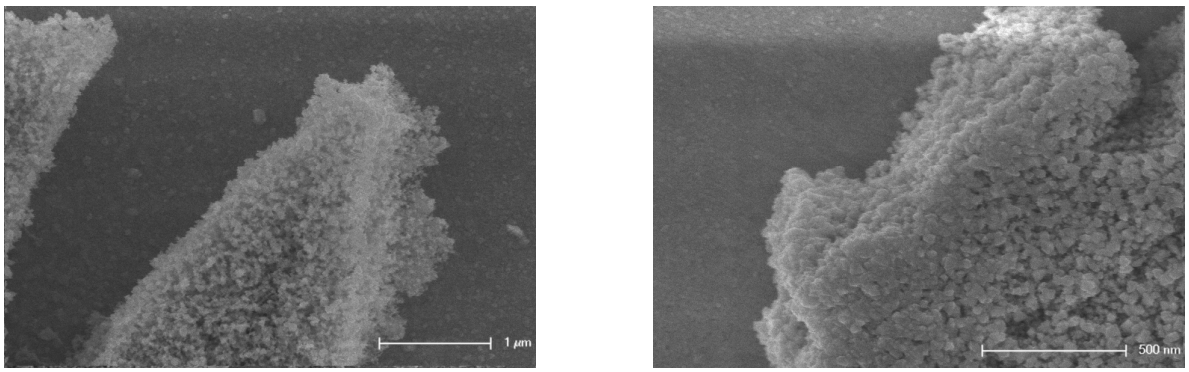

(a) One mud-crack island

(b) Morphology RuOx batch 1

Figure 11: Zoom-in on mud-crack batch 1

Another batch, made with more concentrated precursor, and by using the hotplate as annealing method, showed a brighter shine at x5 magnification, but also, big chunks of dried precursor. After annealing with the hotplate, mud-cracks are visible again, but more interesting, much brighter and rougher RuOx amorphous structure could be noticed at x5 magnification (see fig.12). After re-examining more closely (see fig.13), a complete other morphology, with a rough surface at the µm scale, could be noticed. Unfortunately, it could not be verified with SEM, how the nanoscale morphology turned out.

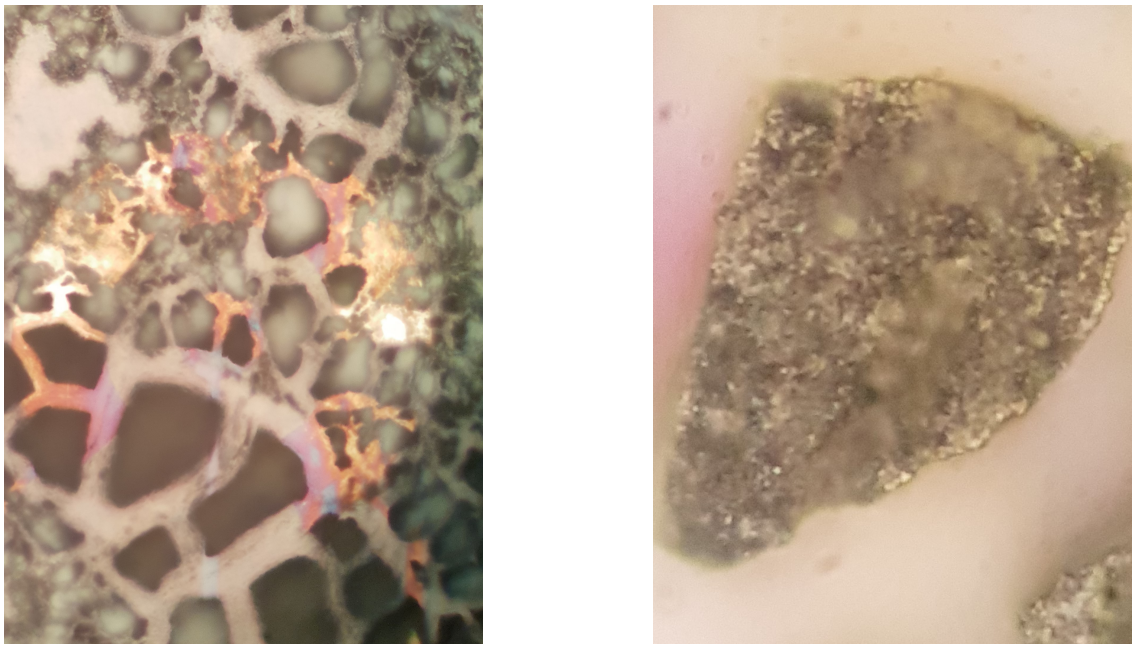

(a) Mud-crack islands (b) One mud-crack island

Figure 12: Zoom-in on mud-crack island batch 2

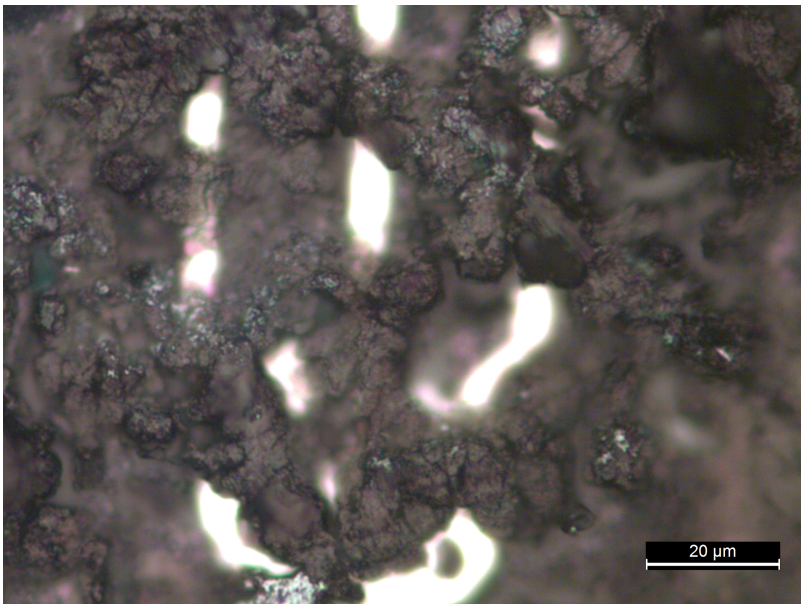

Figure 13: Morphology RuOx batch 2

5.1.2 Electrodeposition

The effectiveness of electrodeposition was also firstly verified by microscope. After the excess solvent from $RuCl_3$ bath was evaporated, the same Ru shiny glow, could be noticed. After baking on the hotplate, the chips were examined under the microscope again. Figure 14a clearly slows crystalline on Pt substrate (white glow). This becomes even more clear if a closer look is taken (see fig.14b). However, after usage in the characterization experiments, the RuOx chip was examined again, and showed a loss in RuOx. This can be seen in picture 15, were now the white color is Pt and dark color RuOx.

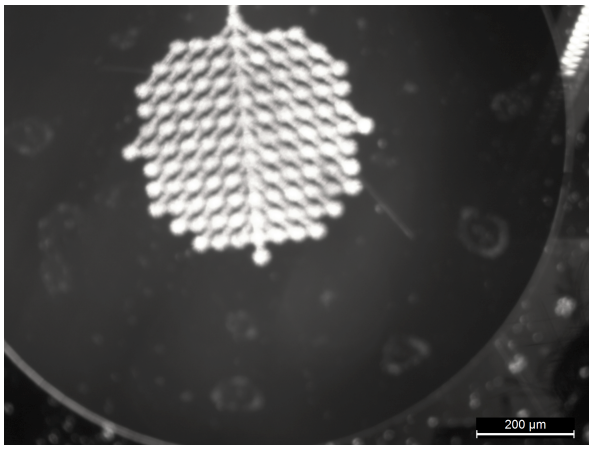

(a) Freshly made RuOx on WE: Bright-field + polarization filter, 5x magnified. Notice the difference in contrast between the Pt CE (grey hemispherical disk
and the RuOx WE(white).

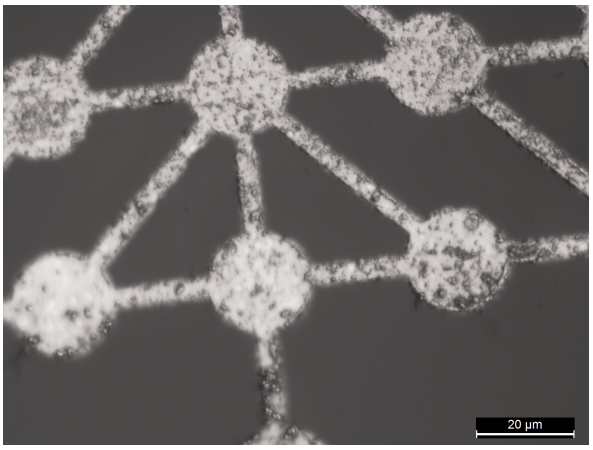

(b) Zoom-in RuOx: Bright-field + polarization filter, 50x magnified.

Figure 14: Electrodeposited 500 micron array

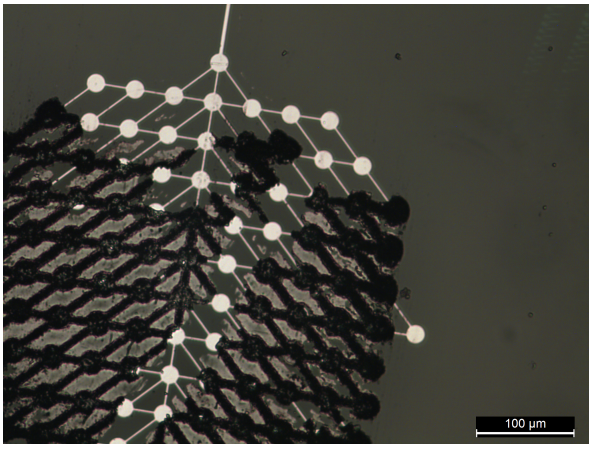

Figure 15: RuOx on WE after usage: Dark-field + polarization filter, 20x magnification. Notice the difference in contrast between Pt(white), and RuOx(black),

Moreover, a few electrodeposited electrode rods of 10 micron were examined. The results can be seen in figure 16, where the black is RuOx and white is Pt. This time it was also chosen to not clean the excess $RuCl_3$ bath solution (black dirt in figure 16). In figure 17, a closer view of the electrodeposited RuOx is shown, which shows yet another morphology in contrast to other production processes, if the distinction is made to look at the RuOx on the Pt only, rather than the RuOx, grown from $RuCl_3$ residue. Unfortunately, there is no comparison with SEM pictures to verify the same morphology on nanoscale.

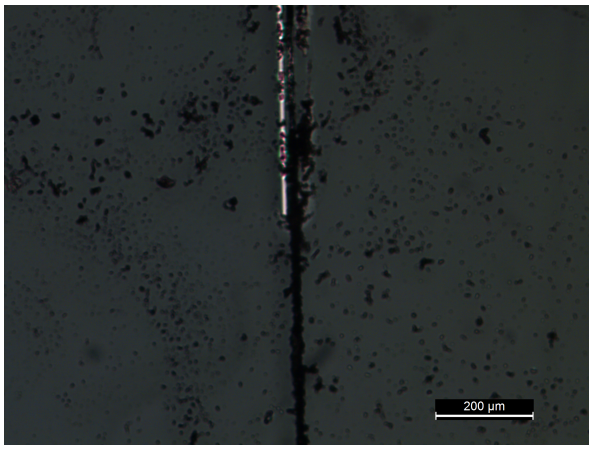

(a) 10 micron wide WE rods: Dark-field + polarization filter, 10x magnification

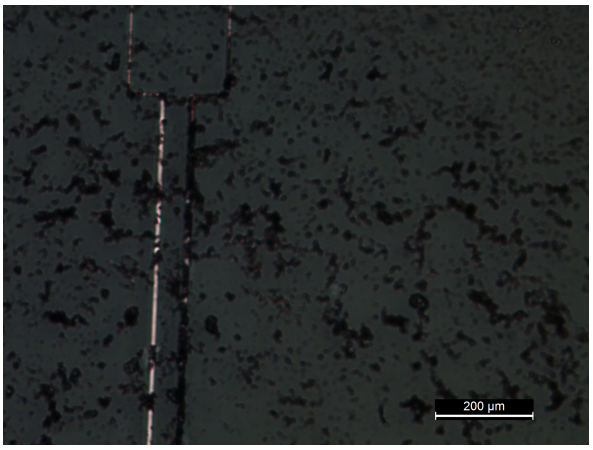

(b) 10 micron wide WE rods: Dark-field + polarization filter, 10x magnification

Figure 16: 10 micron wide rods with: white Pt, Black RuOx WE

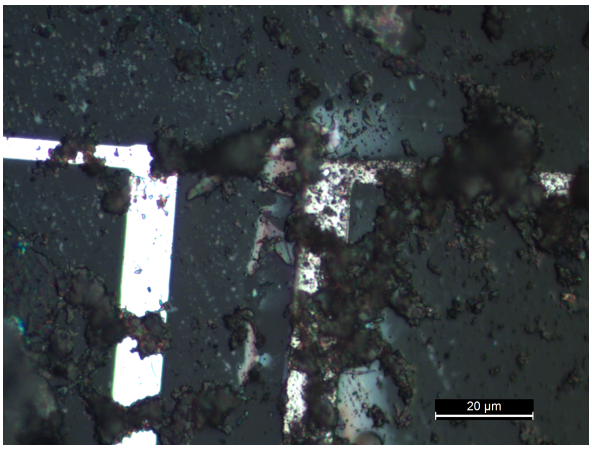

Figure 17: Morphology Electrodeposited RuOx: Dark-field + polarization filter, 100x magnification

5.1.3 Discussion fabrication

In the first batch a noticeable difference with the results of Tanumihardja [9], using the same protocol, is that no RuOx nanorods morphology was noticed. A rather smaller, and more sphere like morphology was noticed (fig.11b) instead. The morphology is very dependent on the production process. Cleanliness of the substrate is the most important factor, regarding RuOx adhesion to the Pt substrate. Even though, all RuOx chips came from one batch, a lot of chips gradually or directly worn out during the characterization process, and some RuOx chips provided the same results in many iterations. This worn out effect, which can be seen in figure 18, could be caused by the pipette flow, since the removal of solution was directly done inside the small hole in the reservoir. By handling the RuOx chips more carefully, and pipetting with less force, the shelf life seem to improve.

The drop-casting method was executable at WE not smaller than 100 micron. Also to effectively cover all of the WE with precursor, a more concentrated solution of $Ru(OH)_3$ in DI is preferred. Because of the difficulty of applying the precursor to the WE, it was chosen that the second batch had all electrodes covered with $Ru(OH)_3$ precursor to ensure all WE of 10, 25, and 50 micron, were exposed to enough $Ru(OH)_3$ precursor. The different RuOx morphology of this batch could be due to a different heating technique/time than the protocol of the first batch.

It would be particularly beneficial to optimize both production protocols used, to guarantee the same quality of each chip. Trying different grain sizes of dissolved $Ru(OH)_3$ in high concentrations already improved results. Also, it seems that the RuOx adheres very poorly to a flat Pt layer. A small oxide layer(mono-layer) on the Pt during the cleaning process is also mentioned [9]. Several

attempts were made improving the adhesion between Pt and RuOx: Roughen up the WE with sand paper, pickle the WE with N,N-dimethylformaldehide, rinse with acetone/water and soap, and etch in 6M HCl. However, non of these methods resulted in a significant improving of the adhesion, rather degrading or even destroy, the thin Pt wires on the glass wafer.

Other, not conducted, but valid options for better adhesion, are: sandblasting the Pt substrate first, use an (conducting) adhesion layer in between Pt and RuOx, and use a different substrate like titanium. Also a different approach of applying the $Ru(OH)_3$ precursor with more force, such as sputtering, can be taken.

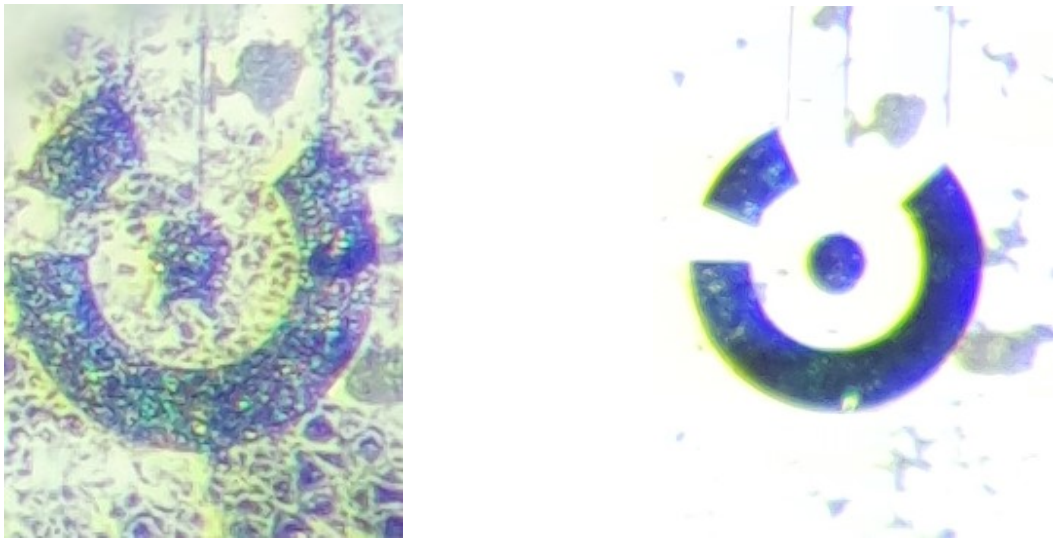

(a) Distinct glow (b) No glow

Figure 18: Left: Fresh RuOx chip, Right: Worn out RuOx chip after several uses

5.2 Characterization experiments

5.2.1 Open circuit potential vs (standard) pH buffers

The first batch of RuOx chips response to hydrogen ion content, in standard buffer solutions of pH 4,7, and 10, is shown in figure 19. All pH calibrations and temperatures can be found in Appendix A.1 table 3. The mean of a minimum of three runs is plotted (using the same RuOx chip), with the error bar representing 1 standard deviation, around each average data point. After applying a linear fit through the average data points, the RuOx chips from 500 until 50 micron show behaviour close to the typical Nernst slope of 59mV/pH. Also, the standard potential E^0 is extrapolated between 600mV and 900mV. The 100 micron performed better than the Nernstian predicted sensitivity, whilst the 10 micron, and 25 micron under performed significantly.

The electrodeposited RuOx chips were tested in the same manner, resulting in figure 20. Both the electroplated RuOx chips have a slope of 50mV/pH, which is again close the the Nernst slope, but still 10% less than the first batch. E^0 is extrapolated between 510mV and 580mV. One alternative shape, the 50 micron rods (w x 100 micron l) has slope of -54 mV/pH and E^0 of around 650mV, which is also near to the anticipated values. It was noticed during the experiments that the electroplated layer of RuOx was very weak, and only one testing run could be conducted before a significant reduction in performance was noticed, therefore only one set of data points(best results) is used.

The second batch of RuOx chips, is again tested in the same manner but with an extended ph range, which can also be found A table 3. The mean of two runs is plotted (using the same RuOx chip), with the error bar representing one standard deviation around one average data point. A linear fit resulted in slopes close to, and above the typical Nernstian slopes. With an extrapolated E^0 between 800mV and 900mV. The 500 micron and 250 micron over performed with 60+/pH, whilst the 10 and 25 micron under performed slightly with 51mV/pH. All OCV vs pH results can be found in Appendix A.2 table 4.

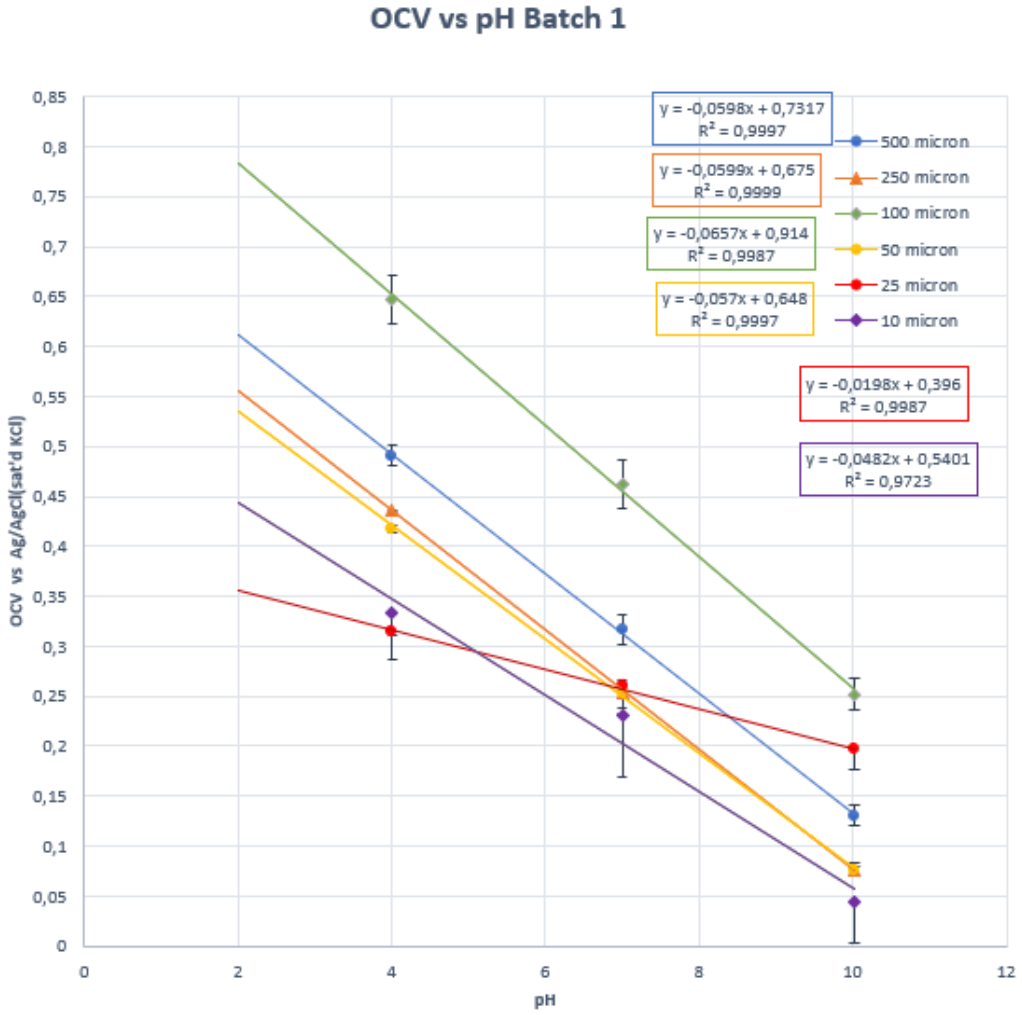

Figure 19: Results OCV batch 1(drop-casted) vs pH: The mean of three runs is plotted, with the error bar representing one standard deviation around one average data point.

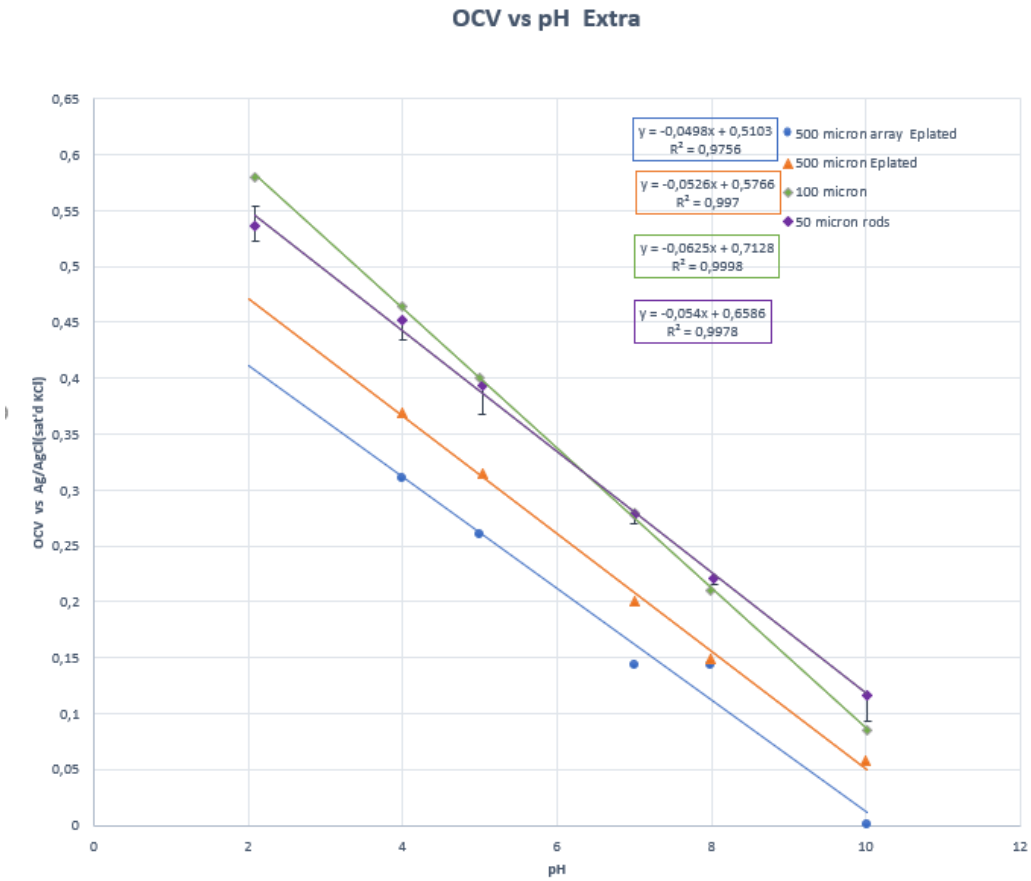

Figure 20: Results OCV vs pH Extra batch(electrodeposited): For the 50 micron rods, the mean of three runs is plotted, with the error bar representing one standard deviation around one average data point. For the electroplated RuOx chips, only one set of data points is used.

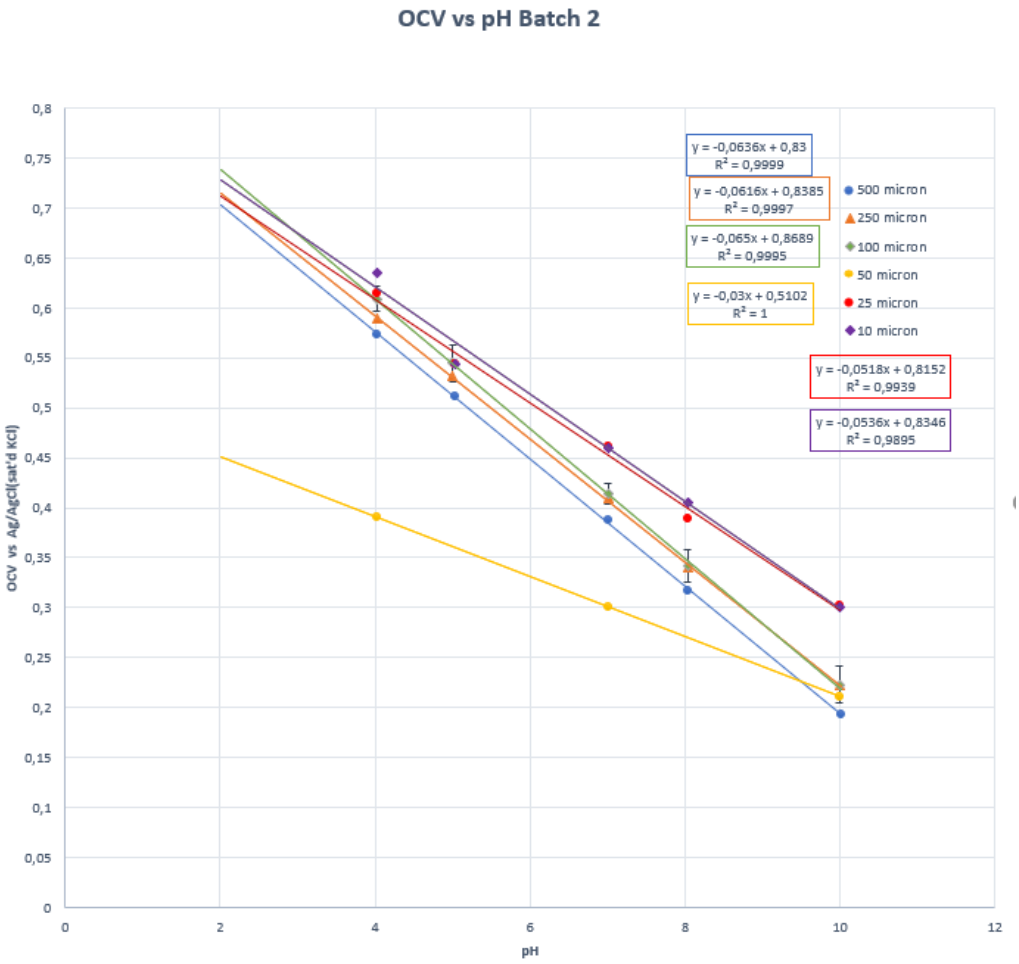

Figure 21: Results OCV batch 2(drop-casted) vs pH: The mean of two runs is plotted, with the error bar representing one standard deviation around one average data point.

5.2.2 Open circuit potential vs drift and influence of oxygen

Two freshly made RuOx chips, 10 micron and 25 micron were used in this test. Deoxygenated PBS buffer (pH 7.4 at 21°C) was pipetted into the reservoir and the recording was started. After a very long time ($+3h$) the measurement was stopped and now oxygen saturated PBS was pipetted into the reservoir. The recording was again executed for $+3h$. The result of the drift slopes can be seen in figure 22. The drift slopes were determined between 1h and 3h, because of the initial drift, and due to one recording stopping early. The results can be seen in table 2.

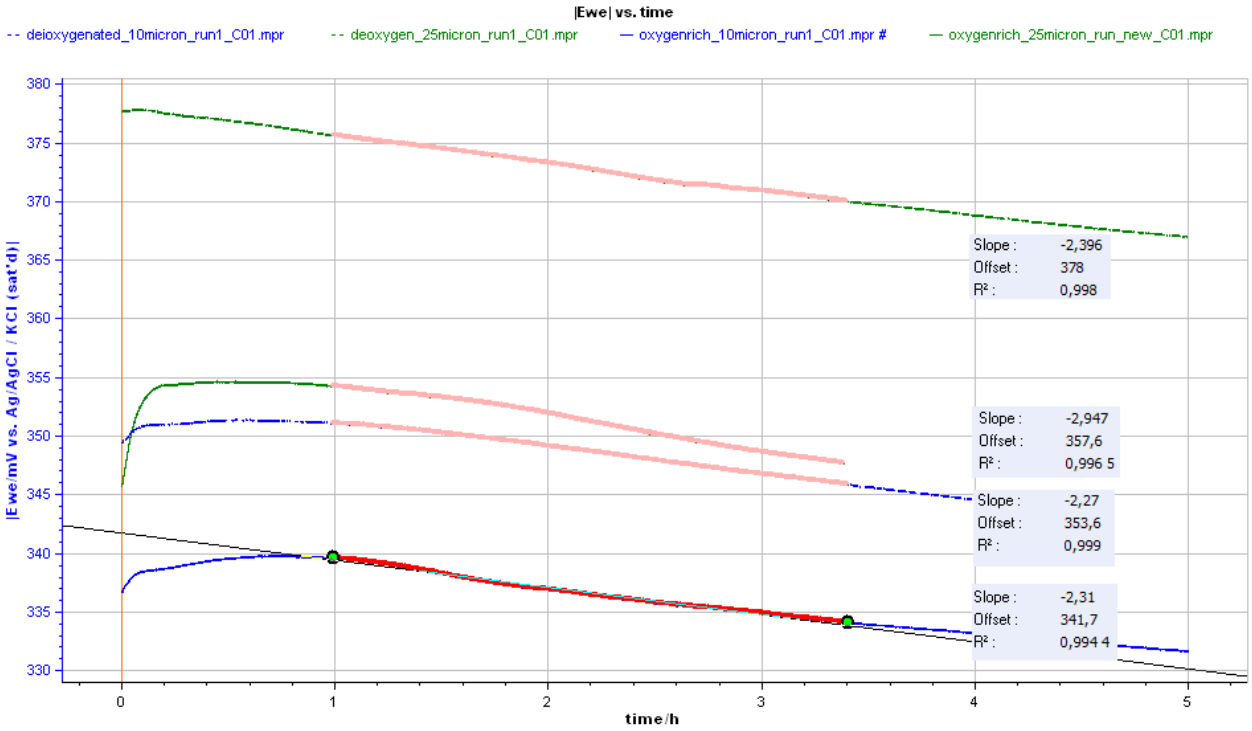

Figure 22: OCV vs drift and influence of oxygen: Green solid line = 25-micron electrode in oxygenated PBS, Green dotted line = 25-micron electrode in deoxygenated PBS, Blue solid line = 10-micron electrode in deoxygenated PBS, Blue dotted line = 10-micron electrode in oxygenated PBS. Also the slopes are given in mV/h with R^2. The offset in mV represents, the PBS buffer OCV at pH 7.4

Table 2: Drift in oxygenated vs deoxygenated state

Chip name	**Drift oxygenated state**	**Drift deoxygenated state**	**Δ Drift**	R^2
10 micron	-2.31 mV/h	-2.27 mV/h	0.04 mV/h	0.99
25 micron	-2.947 mV/h	-2.306 mV/h	0.641 mV/h	0.99

5.2.3 Open circuit potential response time

The recording of the response of a 25 micron RuOx is shown in figure. For the pink and purple lines, the reservoir was half-filled (0.5mL) with 20mM KH_2PO_4, 5mM KCl and 137mM $NaCl$ and at $\sim 50s$ 0.5M K_2HPO_4 was pipetted to fill up the rest of the reservoir (0.5ml). This resulted in a response <10s. At 100s the reservoir was stirred carefully. For the green line the order of adding the solution was reversed and 0.25mL was added on 5s and 50s and was stirred again around 100s. The results were the same as the other recordings.

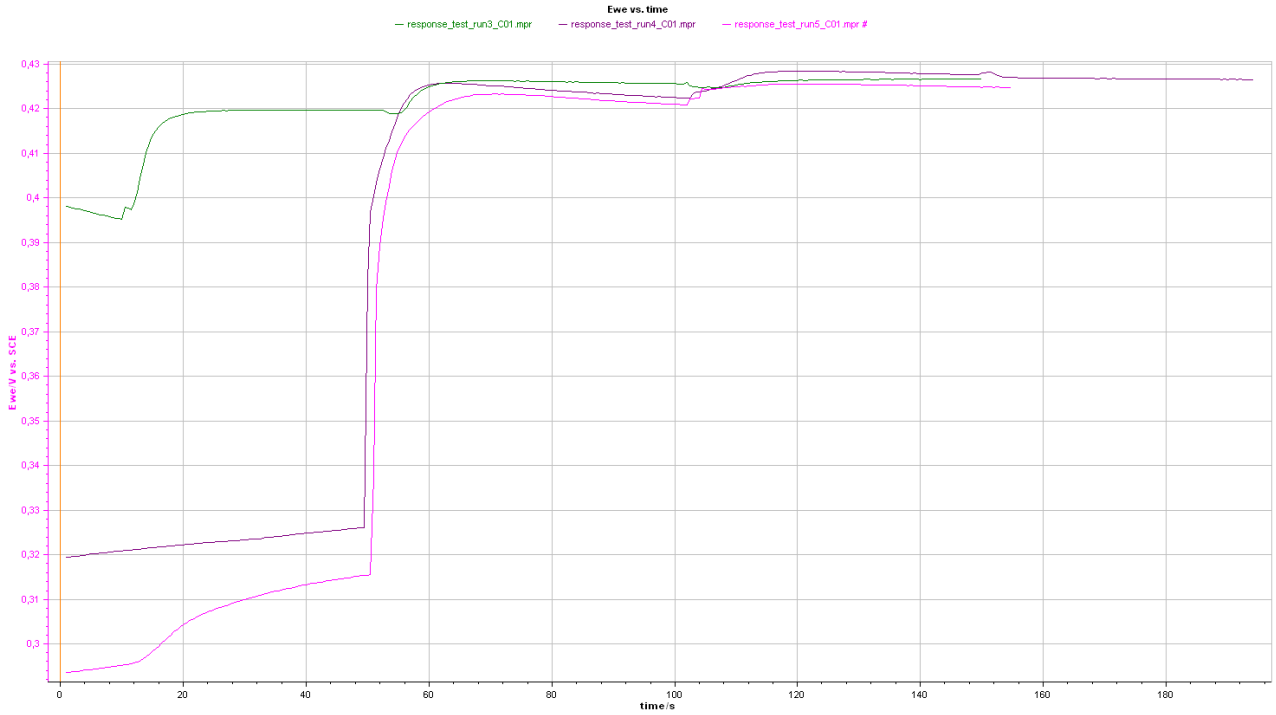

Figure 23: Response time of 25 micron sensor between 2 different plateaus: green = K_2HPO_4 first added, KH_2PO_4, 5mM KCl and 137mM $NaCl$ added second. purple/pink:KH_2PO_4, 5mM KCl and 137mM $NaCl$ added first, K_2HPO_4 added second. Notice the bumb in the pink line at 20s, which is due to a small air bubble leaving the reservoir and extending the exposed WE area

5.2.4 Ohmic drop

Different chips in different solutions were tested for their Ohmic drop. Due to very narrow wires (3 µm) the calculated total resistance of R_w was around 20kΩ, which is in accordance with the measured impedance. Since no dynamic methods were used for elecroanalysis, and the current used in dynamic methods was sufficiently low (nA), no over potentials were noticed. However, due to a higher current density in those small wires electrodepositing was not homogeneous in WE with higher area, but the deposited Ag, seemed to attach better. Some of this effects can be seen in figure 24. Most of the Ag layer was accidentally removed with tape, while the thicker part of the wire (top left fig.24), shows a non-homogeneous Ag layer, which "survived" the tape removal.

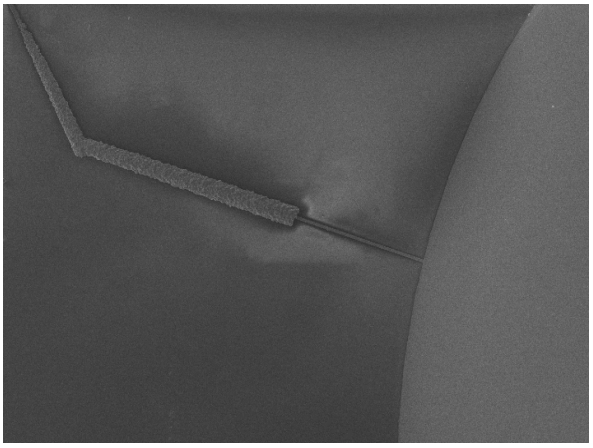

Figure 24: Electroplated Ag on Pt wire (unplated wire is 5 µm thick)

5.2.5 Ag/AgCl QRE characterization

The calibration curve of the Ag/AgCl can be seen in figure 25. The curve shows a good linear nernstian response to Cl^- concentration. However, after using the drop-casting method, the Ag/AgCl layer got removed from the electrode. A little part of the wire (fig.24) survived, which still could be exposed to electrolyte solution. Unfortunately, these results were inconclusive and are not further discussed in this work.

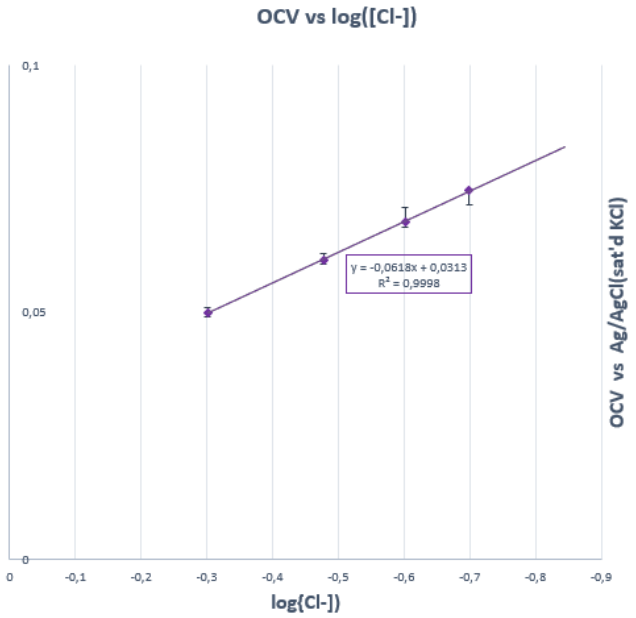

Figure 25: Shows measured OCV vs pCl^-: The error bars represent one standard deviation around each point. The 1M KCl point is omitted, since at 1M the activity coefficient of KCl is >1. (When the point is added the slope becomes 71mV/pCl^-)

5.3 Discussion characterization experiments

5.3.1 pH Response

The first batch clearly shows the potential that miniaturized RuOx sensors have reaching near-nernstian mV/pH slopes. The 10 and 25 micron, under-performed in the first batch, from the results in figure 19 it is clear that the 10 and 25 micron chips had a little to no RuOx modification, still they have a linear response to H^+ activity. The 25 micron initially had better response, but the slope gradually declined each time a measurement was conducted. This decline can be ascribed to the worn out process in figure 18. It was also noticed that a lot of worn out chips had either, no response, a low response ($\sim 10mV$) or still had a mediate ($\sim 30-40mV/pH$), but linear, response to H^+. This effect could be due to another H^+ sensitive chemical compound present which provides a redox potential. The chemical compound present is most likely platinum oxide, with unknown oxide content. This is because in the production process it was already expected that a thin layer of PtO would be present, which inhibits the RuOx to adhere properly. Additionally, PtO is H^+ sensitive which explains the mediate response, this is also confirmed by other works, which state the same mediate response [9,19].

Next, electrodeposition was chosen to get also the smaller chips RuOx modified. The electrodepositing proved to be a more practical method of producing RuOx chips under 100 micron, which performed slightly less, with a lower slope of around 50mV/pH and a standard potential of around 550mV. Nevertheless, the electroplated RuOx chips did not sustain the characterization protocol, this could be due to yet another morphology, which could contribute to these difference in contrast with the drop-casting method.

Overall, different batches resulted in different morphology of RuOx layers, resulting in different OCV slopes. This behaviour is known for hydrous ruthenium oxide [20,21]. and can be described as

follows: Since hydrous RuOx is both a proton and an electric conductor, its electrochemical behaviour at the interface is first prone to the morphology. Hydrous RuOx is described as having different structures, one comprising of a "nano-crystalline", consisting of the nano-rods, also described by Tanumihardja [9], with other regions of rutile-like RuOx and hydrous RuOx clusters [21]. Next, the morphology results in different water behaviour at the interface. Water can either be physisorbed on to the nano-rods or chemisorbed as OHx groups at the interface. [20] Now, the electronic conduction is due to the rutile-like RuOx whilst the proton transport is then due to the water structure at the interface. This basically means that different morphologies result in different ratios in proton, and electron transfer possibilities, which can result in different OCV and standard potentials, response time and cross-sensitivity. If the two drop-casted batches are compared, the only differences are the baking methods, and the different use of $Ru(OH)_3$ precursor concentration. Where the baking time/temperature altered the morphology the most, and the different concentration of precursor resulted in a different amount of RuOx growth. This means the production protocol is of the utmost importance in realizing a morphology, which has the desired response needed for a specific goal, such as the cardiomyocytes studies, in terms of sensitivity, response time and cross-sensitivity. [22]

5.3.2 Drift and Oxygen Sensitivity

The results of the oxygen sensitivity show there is indeed a cross-sensitivity to oxygen content in the solution of as much as 0.6 mV/h between the two oxygen states. All test conducted, showed a less negative drift in deoxygenated state in respect to a more negative drift in oxygenated state. This cross-sensitivity is still not significant, w.r.t. pH measurements, in a time frame of a few hours. Due to the small size of the reservoir (1mL), purging gasses through the solution whilst measuring resulted in unstable graphs, where the drift could not be determined. Therefore it was assumed that deoxygenated PBS and oxygenated PBS would still provide a significant difference in dissolved O_2 concentration during several hours. The initial drift slopes present in the graphs is due to the change of temperature, from being purged with air (7°C), which affects the OCV through the Nernst equation (eq.7), after 1h temperatures were equal to room temperature again, and this was the start of the measuring window. Unfortunately, the oxygen content at that time could not be verified.

5.3.3 Response time

The response time initially could also be seen during the OCV vs pH measurements. When a solution was pipetted into the reservoir, the reaction was instant (<1s). Also from the response time measurement protocol, a rougher estimate of <10s can be concluded, but this response was mainly dependent on how fast the added H^+ ions would diffuse to the the WE, thus was depended on how much force was applied to pipet the solution into the reservoir.

6 Conclusions and Recommendations

Based on all experiments, the Ruthenium oxide sensor has proven to be miniaturiazable to 0.0016 % of the macro-sized sensor developed by Tanumihardja et al. [9], with proof of a Nernstian response of around 59 mV/pH and an extrapolated standard potential close to the one described by the Pourbaix diagram [13]. Morphology is the most important property on electrochemical behaviour at the surface of an electrode, and the response is not effected by the dimensions of the electrode itself. Also drift was not particularly caused by dimensions, but it was mainly caused by a lack of coverage of RuOx on the WE.

The results of oxygen tests have proven an average drift of -2.6 mV/h in PBS, which is 0.04 pH units/h. With a maximum difference of 0.6 mV/h (0.01 pH units/h) between oxygenated, and deoxygenated state. Which proof that for the time frame of 2h, oxygen has no significant impact on the drift. However, the oxygen content was assumed to be around 21%, in oxygenated state and around 5% in deoxygenated state, but this was not quantified, therefore proof of oxygen influence is indefinite and more research should be conducted.

The actual response time was determined at <2s, but couldn't be quantified precisely. It was merely determined by looking at the response of the OCV vs pH measurements. In these measurements it was noticed that after a solution came in contact with the active area of the RuOx sensor, the OCV immediately showed an equilibrium potential. The settling time between two OCV plateaus in the original response test protocol <10s, is therefore limited by mass transport from the bulk to the electrode.

Both production methods proved working RuOx modified pH sensors, with good nernstian behaviour. The drop-casting method was feasible until 100 micron, and electrodeposition proved to be more practical for RuOx chips smaller then 100 micron. Both production methods had a poor adhesion of RuOx to the flat Pt substrate. From all fabricated RuOx chips, only 5% could be used for several iterations without losing any characteristic behaviour.

From the overall results it can be concluded that that macro-sized RuOx is miniaturizable and a suitable competitor for the use as pH sensor in cardiomycytes studies, because of the robustness to oxygen influence.

For future application of the RuOX micro-sensor, it is advisable to further investigate:

i) An optimal production protocol, to ensure the same morphology, and thus behaviour, throughout every production process.

ii) Adhesion of RuOX to the substrate should significantly be improved for micro-sized RuOx sensors. Suggested is to:

- Roughen the surface of the Pt, by sandblasting, or dip etching in HF
- Use an adhesion layer between RuOx and the flat Pt substrate
- Avoid or remove any existing PtO layers, which inhibit RuOx growth/adhesion
- Use alternative substrates like titanium or gold
- Use methods which apply a precursor with more force, such as, sputtering

iii) Conduct more experiments regarding oxygen sensitivity, to rule out significant influence of oxygen.

- An environment can be created which can alter the oxygen content and measure the oxygen content simultaneously

iv) Conduct more experiments with an internal QRE-Ag/AgCl

- For integration purposes it is necessary to have an on-chip QRE, but the behaviour still needs to be characterized

v) Improve the chip design, reducing the ohmic drop of the wires, for proper use in dynamic electrochemical methods

References

[1] M. Keulemans. (2016, Mar.) Cyberorganen. [Online]. Available: https://www.volkskrant.nl/wetenschap/cyberorganen-een-medische-revolutie-in-wording~bf5c758c/?hash=adfb00567f8783f1062dd10e090533e6473606fb

[2] A. D. van der Meer and A. van den Berg, "Organs-on-chips: breaking the in vitro impasse," *Integrative Biology*, vol. 4, no. 5, pp. 461–470, 03 2012. [Online]. Available: https://doi.org/10.1039/c2ib00176d

[3] M. Magazine. (2019, Jan.) Organ-on-a-chip – organs in miniature format. [Online]. Available: https://www.medica-tradefair.com/en/News/Topic_of_the_Month/Topics_of_the_Month_2019/Organ-on-a-chip/Organ-on-a-chip_%E2%80%93_Organs_in_miniature_format

[4] S. N Bhatia and D. E Ingber, "Microfluidic organs-on-chips," *Nature Biotechnology*, vol. 32, pp. 461–470, 08 2014. [Online]. Available: https://doi.org/10.1038/nbt.2989

[5] D. e. a. Huh, "Trends in Cell Biology," *3D Cell Biology*, vol. 21, no. 12, pp. 745–754, 12 2011. [Online]. Available: https://doi.org/10.1016/j.tcb.2011.09.005

[6] M. W. van der Helm, O. Y. F. Henry, A. Bein, T. Hamkins-Indik, M. J. Cronce, W. D. Leineweber, M. Odijk, A. D. van der Meer, J. C. T. Eijkel, D. E. Ingber, A. van den Berg, and L. I. Segerink, "Non-invasive sensing of transepithelial barrier function and tissue differentiation in organs-on-chips using impedance spectroscopy," *Lab Chip*, vol. 19, pp. 452–463, 2019. [Online]. Available: http://dx.doi.org/10.1039/C8LC00129D

[7] S. Głab, A. Hulanicki, G. Edwall, and F. Ingman, "Metal-metal oxide and metal oxide electrodes as ph sensors," *Critical Reviews in Analytical Chemistry*, vol. 21, no. 1, pp. 29–47, 1989, pMID: 28135819. [Online]. Available: https://doi.org/10.1080/10408348908048815

[8] A. Fog and R. P. Buck, "Electronic semiconducting oxides as ph sensors," *Sensors and Actuators*, vol. 5, pp. 137–146, 1984. [Online]. Available: https://doi.org/10.1016/0250-6874(84)80004-9

[9] E. Tanumihardja, W. Olthuis, and A. van den Berg, "Ruthenium oxide nanorods as potentiometric ph sensor for organs-on-chip purposes," *sensors*, vol. 18(9), p. 2901, 2018.

[10] L. R. Faulkner, "Understanding electrochemistry: Some distinctive concepts," *60*, pp. 262–264, 1983.

[11] A. J. Bard and L. R. Faulkner, *Electrochemical Methods.* Wiley, 2000.

[12] P. B. Francesco Basile, G. Fornasari, M. Monti, E. Scavetta, D. Tonelli, and A. Vaccari, "A novel electrochemical route for the catalytic coating of metallic supports," *Studies in Surface Science and Catalysis*, vol. 175, pp. 51–58, 2010.

[13] I. Povar and O. Spinu, "Ruthenium redox equilibria: 3. pourbaix diagrams for the systems ru-h2o and ru-cl–h2o," *Journal of Electrochemical Science and Engineering*, vol. 6, p. 145, 04 2016.

[14] P. Kurzweil, "Metal oxides and ion-exchanging surfaces as ph sensors in liquids: State-of-the-art and outlook," *Sensors*, vol. 9(6), pp. 4955–4985, 2009.

[15] D. A. H.Neil McMurray, Peter Douglas, "Novel thick-film ph sensors based on ruthenium dioxide-glass composites," *Sensors and Actuators B: Chemical*, vol. 28(1), pp. 9–15, 1995.

[16] A. S. Donald Sawyer and J. L. Roberts, *Electrochemistry for Chemists, 2nd ed.* Wiley, 1995.

[17] K.C.Honeychurch, *Printed Films.* Woodhead, 2012.

[18] Z. G. Chen, F. Pei, Y. T. Pei, and J. T. M. De Hosson, "A versatile route for the synthesis of single crystalline oxide nanorods: Growth behavior and field emission characteristics," *Crystal Growth & Design*, vol. 10, no. 6, pp. 2585–2590, 2010. [Online]. Available: https://doi.org/10.1021/cg901558n

[19] C.J.Keattch and J.P.Redfern, "Surface oxidation and reduction of platinum electrodes: Coverage, kinetic and hysteresis studies," *Canadian journal of chemistry*, vol. 46, pp. 875–890, 1967.

[20] J. Heras-Domingo, M. Sodupe, and X. Solans-Monfort*, "Interaction between ruthenium oxide surfaces and water molecules. effect of surface morphology and water coverage," *The Journal of Physical Chemistry*, vol. 123 (13), pp. 7786–7798, 2019.

[21] W. Dmowski*, T. Egami, K. E. Swider-Lyons, C. T. Love, and D. R. Rolison, "Local atomic structure and conduction mechanism of nanocrystalline hydrous ruo2 from x-ray scattering," *The Journal of Physical Chemistry*, vol. 106 (49), pp. 12 677–12 683, 2002.

[22] C.J.Keattch and J.P.Redfern, "The preparation and properties of a hydrous ruthenium oxide," *Journal of the less common metals*, vol. 4(5), pp. 460–465, 1962.

A Appendix

A1. pH Calibrations

Table 3: pH calibrations of different measurements

pH calibration	**Batch 1 (20.5 °C)**	**Batch 2 (21.4 °C)**	**Extra (21.0 °C)**
2	na	na	2.089
4	4.005	4.017	4.005
5	na	5.030	4.997
7	7.00	7.003	7.00
8	na	8.031	7.993
10	10.02	9.992	10.02

A2. OCV vs pH measurement results for different production processes

Table 4: OCV, response, and error for each RuOx chip, whereas: b1=batch 1, b2=batch 2, eplated = electroplated

Chip name	**Standard potential** $E^0(mV)$	**Slope (mV/pH)**	**Error** R^2
500 micron b1	731	-59,8	0,999
500 micron b2	830	-63,6	0,999
500 micron eplated	576	-52,6	0,997
500 micron array eplated	510	-49,8	0,97
250 micron b1	675	-65,7	0,998
250 micron b2	838	-61,6	0,999
100 micron b1	914	-65,7	0,998
100 micron b2	868	-65	0,999
50 micron b1	648	-57	0,999
50 micron b2*	510	-30	1
50 micron rods	658	-54	0,9978
25 micron b1*	396	-19,8	0,998
25 micron b2	815	-51,8	0,9939
10 micron b1*	540	-48,2	0,97
10 micron b2	834	-53,6	0,9895
(*=irregular)			